J. Chem. Sci. (2021) 133:18
https://doi.org/10.1007/s12039-020-01879-x

REGULAR ARTICLE

Crystal structure, characterization and chemical reactivity of novel piperazine derivative ligand for electrochemical recognition of nitrite anion

KHALED AIT RAMDANE[a,b], ACHOUR TERBOUCHE[b,*], CHAFIA AIT RAMDANE-TERBOUCHE[b], HOURIA LAKHDARI[b], KHALDOUN BACHARI[b], HOCINE MERAZIG[c], THIERRY ROISNEL[d], DIDIER HAUCHARD[e] and DJILLALI MEZAOUI[a]

[a]Laboratoire Sciences des Matériaux, Faculté de Chimie, Université USTHB, 16111 Algers, Algeria
[b]Centre de Recherche Scientifique et Technique en Analyses Physico-chimiques (CRAPC), BP384, Bou-Ismail, RP 42004, Tipasa, Algeria
[c]Unité de Recherche de Chimie de l'Environnementet et Moléculaire Structurale, CHEMS, Faculté des Sciences Exactes, Université Frères Mentouri Constantine, Chaabet Ersas, Route Ain El Bey, BP 325, 25017 Constantine, Algérie
[d]CNRS, ISCR (Institut des Sciences Chimiques de Rennes), UMR 6226, Université de Rennes1, 35000 Rennes, France
[e]Institut des Sciences Chimiques de Rennes, UMR CNRS 6226, Ecole Nationale Supérieure de Chimie de Rennes, 11 Allée de Beaulieu, 35708 Rennes, France
E-mail: achour_t@yahoo.fr; achour.terbouche@crapc.dz

MS received 24 August 2020; revised 13 November 2020; accepted 23 November 2020

Abstract. A novel piperazine derivative (3E,3′E)-3,3′-(((piperazine-1,4-diyl bis (ethane-2,1-diyl)) bis (azanediyl)) bis (ethan1-yl-1-ylidene)) bis (6-methyl-2H-pyran-2,4(3H)-dione) (2E-Peaemp) has been synthesized and characterized by ESI-MS, Single-crystal X-ray diffraction, NMR (^{1}H NMR, ^{13}C NMR and 2D NMR), ATR-FTIR, UV-Visible and SEM. The theoretical study of chemical reactivity of 2E-Peaemp was investigated using DFT method. The oxidation-reduction processes and interaction between 2E-Peaemp and nitrite ions were studied using cyclic voltammetry technique. In addition, the detection of NO_2^- was investigated in 0.1 M PBS solution (pH = 7.0) using a carbon paste electrode modified with reduced graphene oxide-graphite carbon/2E-Peaemp system (rGO-GC/2E-Peaemp). XRD study showed that 2E-Peaemp crystallizes in a monoclinic system with $P2_1/c$ space group, and the results obtained from theoretical study well support the experimental results. According to DFT study, HOMO (Highest Occupied Molecular Orbitals)-LUMO (Lowest Unoccupied Molecular Orbitals) energy gap (E_{gap}) and other reactivity descriptors were calculated. The results showed that the ligand exhibits a high chemical reactivity and low kinetic stability. Finally, the cyclic voltammetry measurements showed significant current responses of rGO-GC/2E-Peaemp electrode towards NO_2^- in the concentration range of 0–4 mM with a low limit of detection (LOD = 0.83 μM).

Keywords. Symmetric ligand; Single-crystal X-ray Diffraction; Characterization; DFT; Nitrite detection.

1. Introduction

In recent years, heterocyclic ligands have been widely used in different scientific fields,[1–5] and the majority of drugs developed in the pharmaceutical industry contain molecules of this family of compounds.[6] Bis [3-(1-{[2-(dimethylamino)ethyl]amino}ethyl)-6-methyl-2*H*-pyran-2,4(3*H*)-dione] and its derivatives are interesting ligands due to their variety of potential oxygen and nitrogen donor atoms which can be good chelating agents for metal ions.[7,8] All properties of organic molecules, such as length, geometry and

*For correspondence

Electronic supplementary material: The online version of this article (https://doi.org/10.1007/s12039-020-01879-x) contains supplementary material, which is available to authorized users.

Published online: 09 February 2021

relative position of the donor groups, play a very important role in the production of various hybrid compounds with interesting three-dimensional networks, layers, chains and ribbon structures.[9] These compounds are important flavoring ingredients in food,[10,11] and many metal complexes containing this kind of molecules have been reported for their potential biomedical applications.[12–14]

Among heterocyclic ligands, piperazine is a six-membered ring possessing two nitrogen atoms at opposite positions. Recently, a study performed on the composition of drugs administered orally showed that 60 out of 1000 molecules contain piperazine fragments[15,16] with very interesting biological activities.[17–25] Indeed, to study the structure and the chemical reactivity properties of these organic ligands, various methods of quantum chemistry and molecular modelling techniques have been used.[26–28]

In recent years, various organic molecules were used as sensors for anion recognition such as BF_4^-, $H_2PO_4^-$, I^-[29] F^-, OAc^- and $H_2PO_4^-$.[30] On the other hand, the use of organic molecules to analyze NO_2^- is very rare, except in a few works whose authors were used pyronin[31] and lumimol[32] to detect NO_2^- in solution. However, to our knowledge, there are no works cited in the literature reporting the modified electrodes with piperazine derivatives like 2E-Peaemp, which contains several active sites, to determine nitrite ions in the concentration range of $0 \sim 4$ mM at pH = 7. Indeed, since these species (NO_2^-) are known as undesirable residues in the food chain with potentially carcinogenic effects, the development of simple sensors becomes very important to detect nitrite ions.

To quantify nitrite concentrations, different methods have been developed,[33,34] including chromatographic,[35] spectroscopic[36,37] and electrochemical.[38,39] Among them, electrochemical methods are the most appropriate because of their advantages such as fast response time, inexpensive and effective. In this work, a new piperazine derivative :(3E,3′E)-3,3′-(((piperazine-1,4-diyl bis (ethane-2,1-diyl)) bis (azanediyl)) bis (ethan1-yl-1-ylidene)) bis (6-methyl-2H-pyran-2,4(3H)-dione) was synthesized and characterized by different spectroscopic methods (ESI-MS, ATR-FTIR, NMR, UV-Visible and SEM), cyclic voltammetry and Single-crystal X-ray diffraction analysis. Theoretical calculations at the DFT/B3LYP level of theory, with the standard basis set 6-31G+(d), were employed to understand the chemical reactivity at the atomic level and the structural properties of the synthesized molecule (2E-Peaemp) that could not be found experimentally. Finally, a new electrode based on reduced graphene oxide-graphite carbon/2E-Peaemp system was developed to analyze nitrite ions at pH = 7.

2. Materials and methods

2.1 *Reagents and apparatus*

All reagents and solvents used to prepare the measurement solutions were of the highest purity and analytical grade from Sigma–Aldrich or Fluka chemicals Company and the different solutions were prepared in free CO_2 deionised water. XRD data were collected on a D8 Venture Bruker AXS diffractometer equipped with a CMOS PHOTON 100 detector, Mo-$K\alpha$ radiation (λ = 0.71073 Å and multilayer monochromator at 150 K. SEM characterization and ESI-MS (Positive ion electrospray ionization mass spectrum) were performed using LC/MS-MS Agilent Technologies' spectrometer and a scanning electron microscope FEI QUANTA 250, respectively. ATR-FTIR spectrum was realized on a Bruker LPHA-T spectrometer, and all ^{1}H NMR, ^{13}C NMR and 2D NMR measurements were recorded at 25 °C on a Bruker 400 Avance III HD spectrometer. UV-Visible spectrum was recorded on a SPECORD plus spectrophotometer in the range 200–1000 nm. DFT calculations and electrochemical measurements were carried using DFT/B3LYP/6-31G+ (d) level of theory and Potentiostat/Galvanostat Metrohm Autolab 302N, respectively.

2.2 *Synthesis of ligand*

The new ligand ((3E,3′E)-3,3′-(((piperazine-1,4-diyl bis (ethane-2,1-diyl)) bis (azanediyl)) bis (ethan1-yl-1-ylidene)) bis (6-methyl-2H-pyran-2,4(3H)-dione)) was synthesized by adding 1.72 mL of 2,2′-(piperazine-1,4-diyl) bis (ethan-1-amine) (10 mmol) to 20 mmol (3.36 g) of dehydroacetic acid dissolved in 20 mL of absolute ethanol. Then, the mixture was stirred for 24 h, and a white precipitate was formed, collected by filtration and washed with ethanol. The single crystals of the product (2E-Peaemp) were obtained after refluxing in hot dichloromethane, according to the reaction mechanism that describes the synthetic pathway for the formation of 2E-Peaemp (Scheme 1). This synthesis was obtained by a nucleophilic attack of NH_2 group on the extracyclic carbonyl of dehydroacetic acid followed by the elimination of two molecules of water. The formed crystals are insoluble in acetone, ethanol, water and dichloromethane

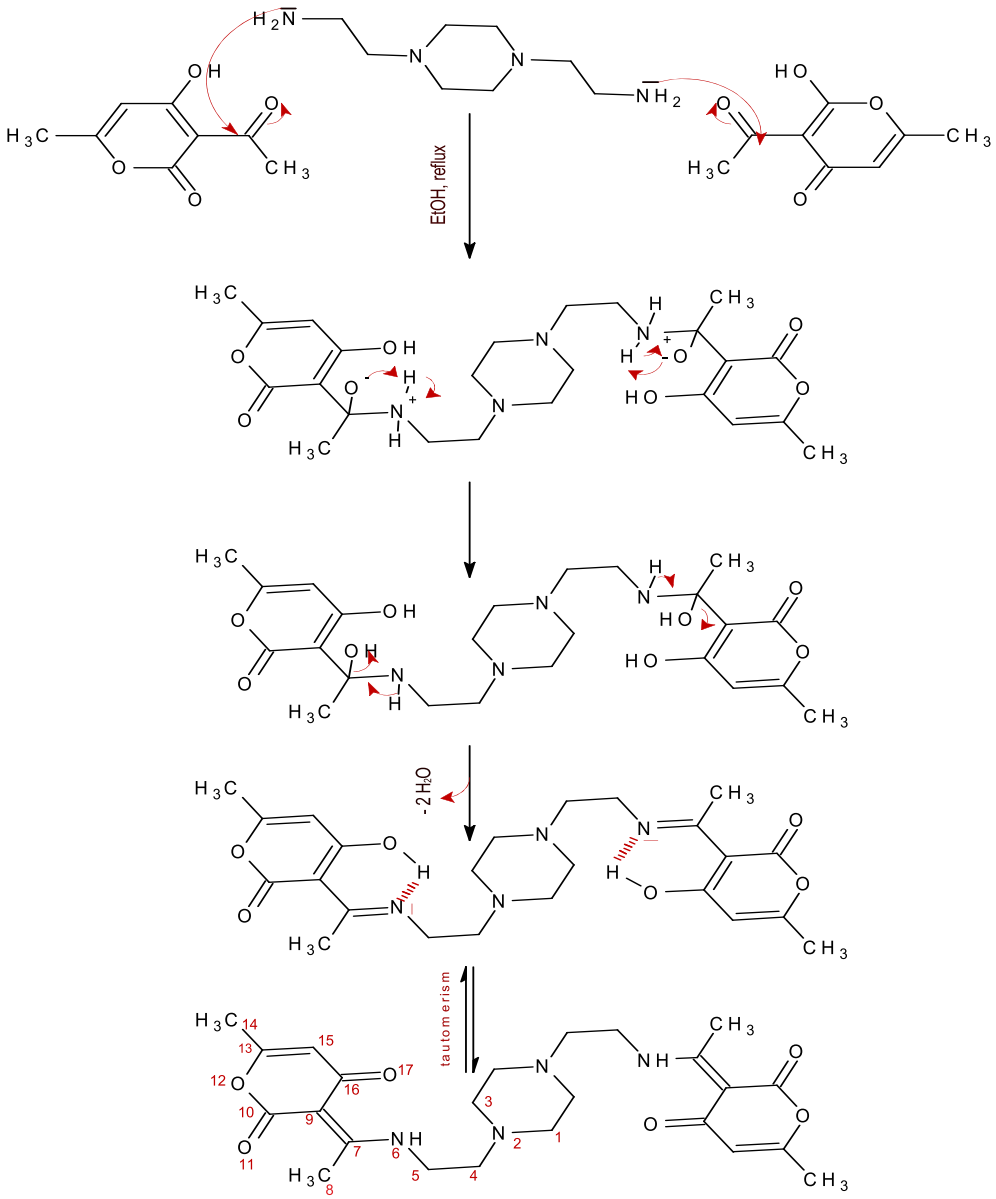

Scheme 1. Proposed mechanism for the formation of 2E-Peaemp.

(DCM). However, it is soluble in hot chloroform ($CHCl_3$) and dimethylsulfoxide (DMSO). The characterization results of 2E-Peaemp are as follows:

Yield: 63% (2.977 g); M.p. 230 °C. **ESI-MS** (in H_2O (0.1% HCOOH/CH_3CN (50%/50%): m/z found (calc.): 473.100 (473.534) $[M+H]^+$; 237.100 (237.267) $[M/2+H]^+$, with ($M=C_{24}H_{32}N_4O_6$) (M refers to the molecular weight of Ligand). **^{1}H NMR (400 MHz, $CDCl_3$, 25 °C, ppm, δ)**: 2.12 (s, 6 H_{14}, CH_3); 2.60 (s, 8 $H_1$and H_3, CH_2); 2.65 (s, 6 H_8, CH_3); 2.68–2.71 (t, *J*/Hz 6.2, 4 H_4, CH_2); 3.53–3.58 (dd, *J*/ Hz 11.4, 5.8 Hz, 4 H_5, CH_2); 5.65 (s, 2 H_{15}, CH); 14.05 (broad s, 2N*H*). **^{13}C NMR (101 MHz, $CDCl_3$, 25 °C, ppm, δ)**: 18.49 (C_8); 19.76 (C_{14}); 41.65 (C_5); 52.91 ($C_1$and C_3); 55.90 (C_4); 96.66 (C_9); 107.50 (C_{15}); 162.46 (C_{13}); 163.91 (C_{10}); 175.46 (C_7); 184.51 (C_{16}). **HSQC NMR (101 MHz, $CDCl_3$, 25 °C, ppm, δ)**: 2.12:19.76 (H_{14}: C_{14}); 2.60:52.91 (H_1:C_1) and (H_3:C_3); 2.65:18.49 (H_8:C_8); 2.68:55.90 (H_4:C_4); 3.53:41.65 (H_5:C_5); 5.65:107.50 (H_{15}:C_{15}). **HMBC NMR (101 MHz, $CDCl_3$, 25 °C, ppm, δ)**: 2.12:107.50:162.46 (H_{14}:C_{15}:C_{13}); 2.60:55.90 (H_1:C_4); 2.65:96.66:175.46 (H_8:C_9:C_7); 2.68:41.65 (H_4:C_5:C_7); 3.53:55.90 (H_5:C_4:C_7); 5.65:19.76:96.66:162.46:184.51 (H_{15}:C_{14}:C_9:C_{13}:C_{16}). **UV-Vis (DMSO, λ :nm (ε :L mol^{-1} cm^{-1})**: 201 nm (ε= 13379.61 L mol^{-1} cm^{-1}); 247 nm (ε= 4417.52 L mol^{-1} cm^{-1}); 315 nm (ε= 5427.46 L mol^{-1} cm^{-1});

384 nm (ε= 3039.9 L mol^{-1} cm^{-1}). **ATR: cm^{-1}**: 3088 υ(N-H); 2949 υCH (CH_3); 2833 υCH (CH_2); 2802 υCH (CH); 1689 υ(O–C=O); 1665 υ(C–C=0); 1577 δ(N–H).

3. Results and Discussion

3.1 *Characterization of the ligand*

3.1a *X-ray crystallography of the ligand*: Well-defined colorless crystals with a size of about 0.550 x 0.370 x 0.340 mm^3 have been selected and mounted on a cryoloop for X-ray diffraction analysis. Crystal data for 2E-Peaemp showed that the ligand crystallizes in monoclinic system and space group P $2_1/c$, with the lattice parameters of a = 7.3809(9) Å, b = 13.2331(14) Å and c = 12.0852(15) Å. A total of 10330 reflections were collected, of which 2609 were independent (R_{int} = 0.0336). The final refinement converged to R value of 0.0434 [$I > 2\sigma(I)$] and wR = 0.1162 (all data). An ORTEP representation of ligand is shown in Figure 1a. In addition, the crystal data, the conditions of X-ray data collection, isotropic and anisotropic displacement parameters are summarized in Tables S1–S4, Supplementary Information.

In the view of the ligand's crystalline packing along (100) shown in Figure 1b, the parameters of C–H—O and C–H—N hydrogen bonds (length and binding angles) are collected in Table S5, Supplementary Information. The results showed that there are several inequivalent hydrogen bonds in the crystal of 2E-Peaemp: the shortest are C15-H15…O17 (2.4594 Å)

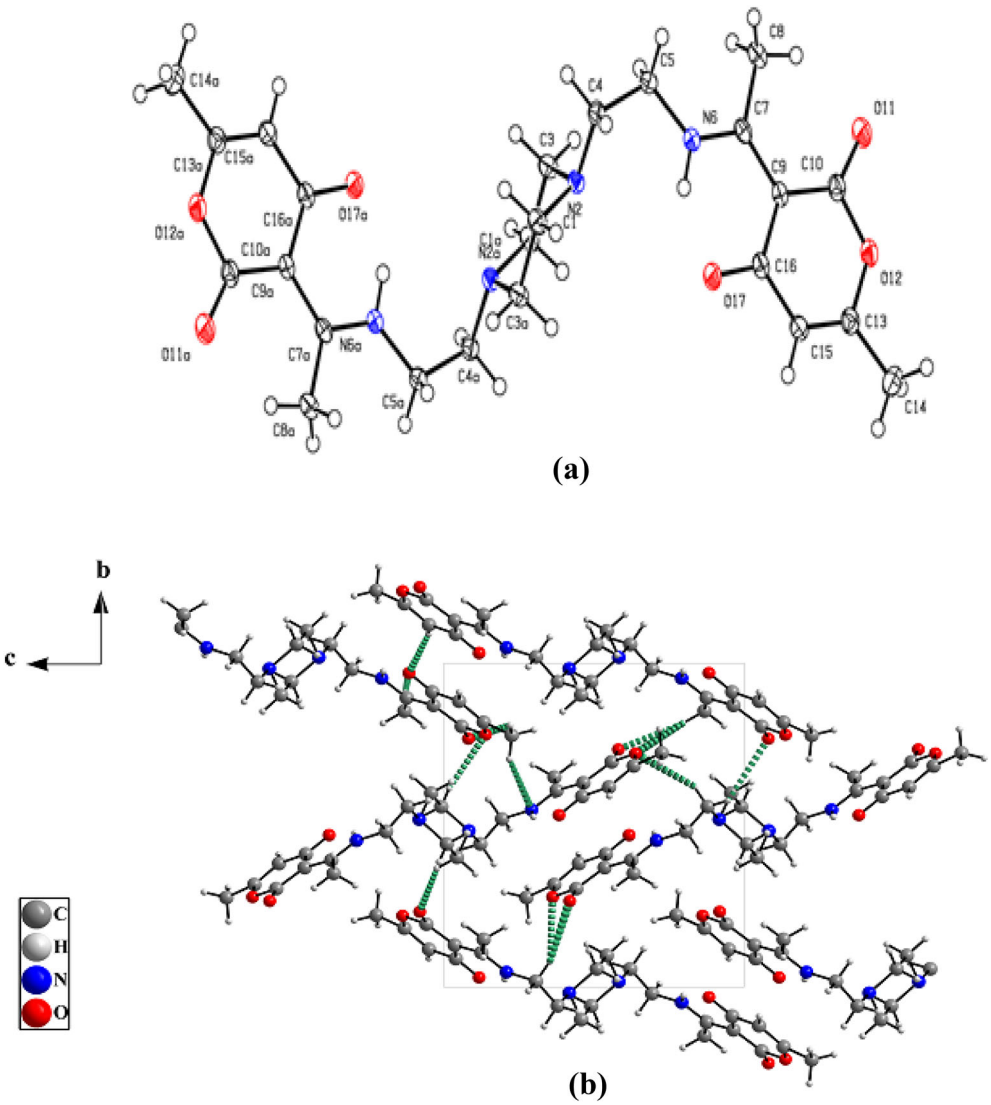

Figure 1. Molecular Structure of ligand: (a) ORTEP representation; (b) Crystal packing view of 2E-Peaemp.

and C8-H8A…O12 (2.6994 Å), while the longest are C4-H4B…O11 and C5—H5A—O11 with hydrogen bond distance of 2.9876 Å and 2.9529 Å, respectively. These hydrogen bonds are responsible for the potential stabilization of the formed molecule.

3.1b *Mass spectrometry (ESI-MS)*: The mass spectrum of 2E-Peaemp recorded in H_2O (0.1% Formic acid)/Acetonitrile (50%/50%) (Figure S1, Supplementary Information) showed molecular ion peaks assigned to the molecular weight of the ligand. The peak at m/z found (calc.): 473.100 (473.534) with high relative abundance corresponds to $[M+H]^+$ (M = $C_{24}H_{32}N_4O_6$) (M refers to the molecular weight of ligand). On the other hand, the second molecular ion peak at m/z 237.100 (237.267) is assigned to $[M/2+H]^+$. The presence of these fragments confirms the structure of the ligand.

3.1c *Infrared spectrometry*: The ATR-FTIR spectrum of the ligand (Figure S2, Supplementary Information) shows a band at 3088 cm^{-1} associated with the stretch vibration of the NH group.[40] The two intense peaks observed at 1689 and 1665 cm^{-1} are attributed to the stretching vibration of O–C=O (Lactone) and C–C=O groups, respectively.[41,42] While, the peak appeared at 1577 cm^{-1} is attributed to NH deformation vibration (δNH). The pyrazine ring showed C–N and C–C stretching vibrations at 1357 cm^{-1} and 1591 cm^{-1}, respectively.[43–45] The peaks at 2949 cm^{-1}, 2833 cm^{-1} and 2802 cm^{-1} are due to the stretching vibration $\upsilon_{C\text{-}H}$ in CH_3, CH_2 and CH groups, respectively, and the band observed at 1466 cm^{-1} is related to the C=C bond stretching vibration (υC=C). In contrast, the remaining bands localized between 1000 cm^{-1} and 700 cm^{-1} are assigned to the out-of-plane bending modes C=C, C–N and C–C of the heterocycle.[24]

3.1d *NMR spectrometry*: NMR spectroscopy is a powerful technique that provides detailed information about the structure of the ligand. Knowing that the ligand is symmetrical, its NMR spectra show the appearance of half number of protons and carbons. The experimental results obtained by ^1H NMR spectroscopy (Figure S3a, Supplementary Information) showed two singlet peaks at 2.12 and 2.65 ppm, corresponding to three protons of each CH_3 group (s, H_{14} and H_8, CH_3). Between these signals, we observe an intense singlet peak attributed to the eight protons of four CH_2 of the piperazine cycle at 2.60 ppm (s, 4 H_1 and 4 H_3, CH_2). The triplet signal between 2.68 and 2.71 ppm corresponds to the equivalent protons (4 H_4) of the extracyclic methylene with coupling constant $^3J_{H–H}$/=6.2 Hz (calculated $^3J_{H–H}$ =8 Hz). The methylene at position 5 appears as a doublet of doublet signal at 3.53–3.58 ppm, with coupling constant $^3J_{H–H}$=11.4 and $^3J_{H–H}$=5.8 Hz (calculated $^3J_{H–H}$=12 Hz, $^3J_{H–H}$=8 Hz), due to the adjacent NH and CH_2 groups. The singlet peak at 5.65 ppm is attributed to H_{15} proton, and the broad singlet signal showed at 14.05 ppm corresponds to the hydrogen atom directly attached to nitrogen of NH group. Furthermore, the ^{13}C NMR spectrum (Figure S3b, Supplementary Information) showed 11 signals representing 22 carbon atoms appeared between 18 and 184 ppm, corresponding to C_8, C_{14}, C_5, C_1, C_3, C_4, C_9, C_{15}, C_{13}, C_{10}, C_7 and C_{16}.

All proton and carbon atoms have been precisely attributed based on 2D NMR analysis cross-peak correlations. In fact, the HSQC NMR spectrum (Figure S4a, Supplementary Information) indicated the direct correlation between protons and their associated carbons. Therefore, the appearing cross-peaks correspond to 2.12:19.76 (H_{14}:C_{14}); 2.60:52.91 (H_1:C_1 and H_3:C_3); 2.65:18.49 (H_8:C_8); 2.68:55.90 (H_4:C_4); 3.53:41.65 (H_5:C_5) and 5.65:107.50 (H_{15}:C_{15}). On the other hand, the HMBC NMR spectrum (Figure S4b, Supplementary Information) showed obvious coupling with long-range connectivity between protons and neighboring carbons and all quaternary carbons: 2.12:107.50:162.46 (H_{14}:C_{15}:C_{13}); 2.60:55.90 (H_1:C_4); 2.65:96.66:175.46 (H_8:C_9:C_7); 2.68:41.65 (H_4:C_5:C_7); 3.53:55.90 (H_5:C_4:C_7) and 5.65:19.76:96.66:162.46:184.51 (H_{15}:C_{14}:C_9:C_{13}:C_{16}).

3.1e *UV-Visible spectrophotometry*: The electronic spectrum was recorded between 200 nm and 600 nm in chloroform (Figure S5, Supplementary Information) in the presence of 10^{-5} M of ligand (ℓ=1 cm). Four bands assigned to $\pi\rightarrow\pi^*$ and $n\rightarrow\pi^*$ transitions appeared around the range of 201–384 nm.[46] The bands observed at 201 nm and 247 nm are assigned to C=C transition, and those located at 315 nm and 384 nm are attributed to C=O groups.

3.1f *Surface morphology*: Through scanning electron microscopy, beautiful homogeneous monoclinic prismatic crystals of the same size well defined were reported in Figure S6, Supplementary Information. The recorded SEM image showed that the ligand exhibits a uniform crystal structure in its crystal lattice. In addition, SEM micrograph of this compound revealed that the structure of the crystal has variable lateral dimensions.

3.2 *Quantum chemical calculations*

The theoretical parameters of the ligand were calculated with theoretical DFT using Gaussian 09,[47] involving the well-known Becke-three-parameter Lee-Yang-Parr function (B3LYP) with 6-31G+(d) level of theory in the vapor phase. The experimental parameters (XRD) and the optimized geometric parameters (DFT; Figure 2a), such as bond lengths, bond and torsion angles were calculated and shown in Table S2, Supplementary Information. By neglecting the signal of the dihedral angle values (torsion angles),[48] a potential agreement between the experimental and theoretical results has been obtained.

3.2a *Chemical reactivity*: The HOMO and LUMO are useful to determine the different electronic and optical properties of molecules.[49] The HOMO-LUMO energy gap of the molecule as well as ionization potential (I.E), electron-affinity ionization energy (E.A), energy gap (gap), chemical potential (μ), electronegativity (χ), chemical hardness (η), chemical softness (S) and electrophilicity index (w) are useful for understanding the chemical reactivity of molecules at the atomic level.[50,51]

The reactivity parameters (global reactivity descriptors) given in Table 1 were calculated using the following equations:

$$\chi = \frac{\text{I.E} + \text{E.A}}{2}, \quad \mu = -\frac{\text{I.E} + \text{E.A}}{2},$$
$$\eta = \frac{\text{I.E} - \text{E.A}}{2}, \quad s = \frac{1}{2\eta}, \quad w = \frac{\mu^2}{2\eta}$$

According to Figure 2b, the spatial distribution of the LUMO is mainly delocalized over the π system of (3*E*)-3-(1-aminoethylidene)-6-methyl-2*H*-pyran-2,4(3*H*)-dione group (derivative dehydroacetic acid) and the free electronic doublet of the nitrogen atom of –NH group of the molecule. The occupied frontier orbitals (HOMO) is located over the π system of (3*E*)-3-(1-aminoethylidene)-6-methyl-2*H*-pyran-2,4(3*H*)-dione and on half of the piperazine cycle. It should be noted that the HOMO involves predominantly the π system and the electronic density of 2E-Peaemp.

The HOMO-LUMO gap is 4.569 eV and ionization potential and electron-affinity ionization energy are I.E = − E_{HOMO} = 6.271 eV and E.A = − E_{LUMO}= 1.702 eV, respectively. Knowing that the soft molecule is characterized by low hardness, high softness, small energy gap and excitation energies,[45] so this molecule will react by interference between the wave functions of their HOMO and LUMO orbitals and their electron densities, involving easy modifications to be more reactive. The remarkable values of chemical potential and electrophilicity index indicate that the electrons tend to escape into the molecule. In addition,

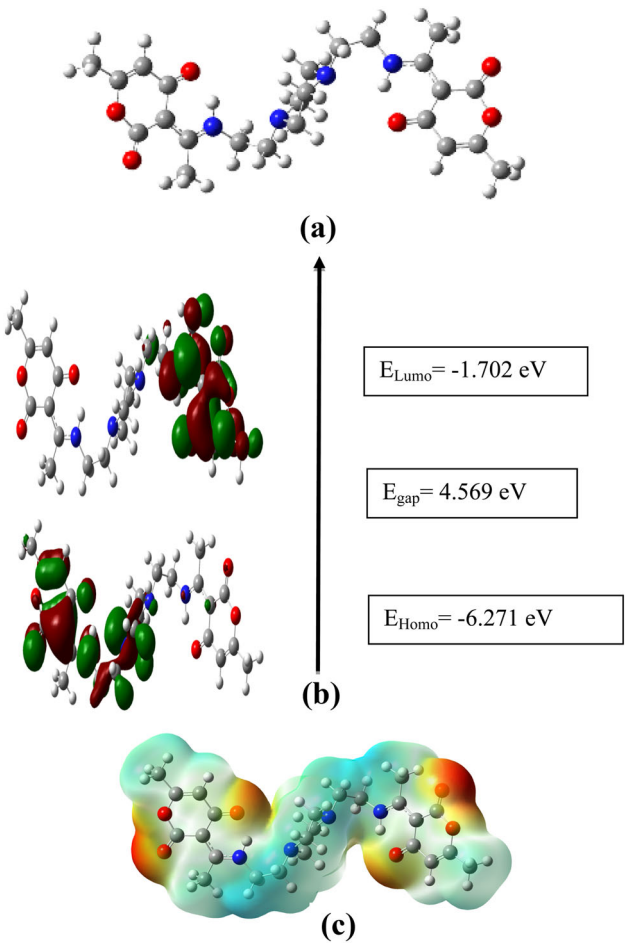

Figure 2. Optimized geometry diagram of 2E-Peaemp: (a) Optimized structure view; (b) Frontier molecular orbitals (HOMO and LUMO); (c) Molecular electrostatic potential (MEP).

Table 1. Global reactivity descriptors (eV) for 2E-Peaemp by DFT/B3LYP/6-31 + G(d) method.

Reactivity descriptors	2E-Peaemp
|ΔE| (Gap/HOMO-LUMO)	4.569
Ionization potential (I.E)	6.271
Electronic affinity (E.A)	1.702
Electronegativity (χ)	3.987
Chemical potentiel (μ)	− 3.987
Chemical hardness (η)	2.284
Chemical softness (S) $(eV)^{-1}$	0.437
Electrophilicity index (ω)	3.479
Dipole moment (D)	1.312

the chemical activity parameters reported in Table 1 showed that the ligand presents an electrophilic (high electrophilicity) and nucleophilic (high electronegativity) characters, involving complexation with various species. These results revealed that the ligand exhibits high chemical reactivity and low kinetic stability. On the other hand, the global reactivity descriptors are calculated in order to evaluate the nature of this ligand (electrophilic and nucleophilic (by C=O and C-O-C groups)). Indeed, it is precisely because of the electrophilic nature of the ligand that we decided to make an application to detect NO_2^- ions (NO_2^--2E-Peaemp interaction via –NH groups after protonation) (see the reaction mechanism in section 3.3.2).

3.2b *Molecular electrostatic potential (MEP)*: Molecular electrostatic potential was evaluated using the B3LYP/6-31+G(d) method. This technique gives information about the total charge distribution of molecules. While MEP map was investigated to identify the reactive sites of electrophilic and nucleophilic attacks on the functional groups present in the studied molecule.

According to the calculations, the MEP map shows different regions (Figure 2c): those colored in red and yellow correspond to electron-rich, while the blue region corresponds to electron-poor sites (nucleophilic attack). MEP map showed that the maximum negative surface potential (red or yellow) was located on the oxygen atoms and the positive regions (blue) were observed mainly on the hydrogen atoms of ligand (2E-Peaemp). The high electronegativity of –C=O and –C–O–C– groups present the most suitable sites for the electrophilic attack of 2E-Peaemp. Whereas, the blue region represents the site of the highest reactivity to nucleophilic attack.

3.3 *Electrochemical study*

3.3a *Electrochemical behavior of ligand*: The electrochemical behavior of the ligand was studied in DMSO and tetrabutylammonium hexafluorophosphate (TBAPF6) at 20 $mV.s^{-1}$ scan rate by cyclic voltammetry using a platinum wire, glassy carbon and saturated Ag/AgCl as working electrode, a counter electrode and reference electrode, respectively. The voltammogram of the ligand (Figure S7, Supplementary Information) showed two cathodic waves associated to two anodic waves observed at Ep_{a1}=0.86 V (Ep_{c1} = 0.92 V) and Ep_{a2}=0.36 V (Ep_{c2} = − 0.56 V). These peaks are attributed to the oxidation-reduction process of C=O and NH groups, respectively.[52]

3.3b *Nitrite analysis*: The electrocatalytic behavior of the modified electrode (rGO-GC/2E-Peaemp) towards nitrite determination was investigated by cyclic voltammetry (CV) at various concentrations of nitrite, and the oxidation currents of nitrite ions were recorded at room temperature at a potential scan rate of 20 mV s^{-1}. The modified carbon paste electrode was prepared by adsorption of a solution of 10 mg of 2E-Peaemp in 5 mL of dimethyl sulfoxide on a compound containing 100 mg of reduced graphene oxide and 100 mg of graphite powder for 24 h, and then the mixture was filtered and washed with distilled water several times. The resulting product was dried in an oven at 60 °C and mixed with few drops of paraffin oil to obtain a uniform paste. Finally, this paste is inserted into a 2 mm diameter glassy tube. The cyclic voltammograms obtained using the modified electrode (rGO-GC/2E-Peaemp) in 0.1 M PBS solution (pH = 7.0) in the absence and the presence of nitrite are reported in Figure 3.

The electrochemical behavior of nitrite ions on this electrode showed an oxidation wave around 0.8 V, attributed to the oxidation peak of nitrite[53–55] which is close to the oxidation potential of the ligand (0.83 V) observed on rGO-GC/2E-Peaemp in PBS buffer solution. Figure 3 clearly shows the current response of the rGO-GC/2E-Peaemp electrode towards nitrite oxidation. The electrocatalytic behavior of 2E-Peaemp towards oxidation of nitrite (Figure 4) revealed that

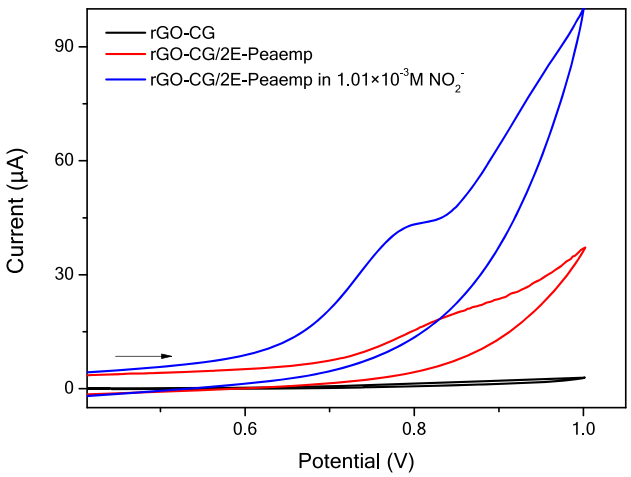

Figure 3. Cyclic voltammograms recorded on rGO-GC/2E-Peaemp electrode in 0.1 M PBS solution in the absence and the presence of 0.00101M NO_2^- (V vs. saturated Ag/AgCl working electrode).

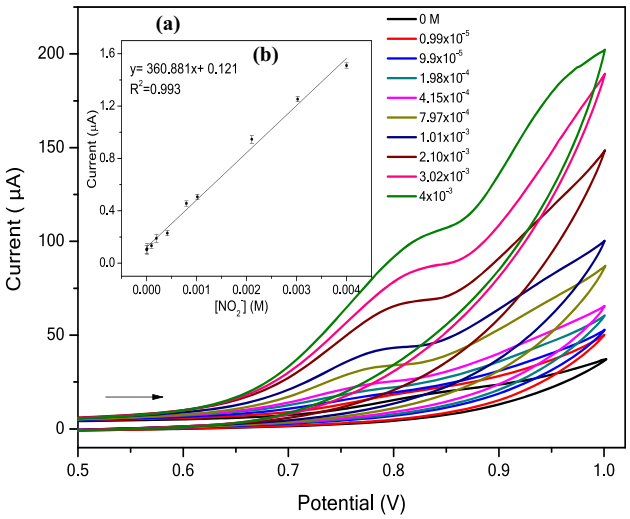

Figure 4. (a) Amperometric response of rGO-GC/2E-Peaemp modified electrode vs. concentration of nitrite in PBS (pH = 7); (b) Calibration plot of current response vs. concentration of NO_2^- (V vs. saturated Ag/AgCl working electrode).

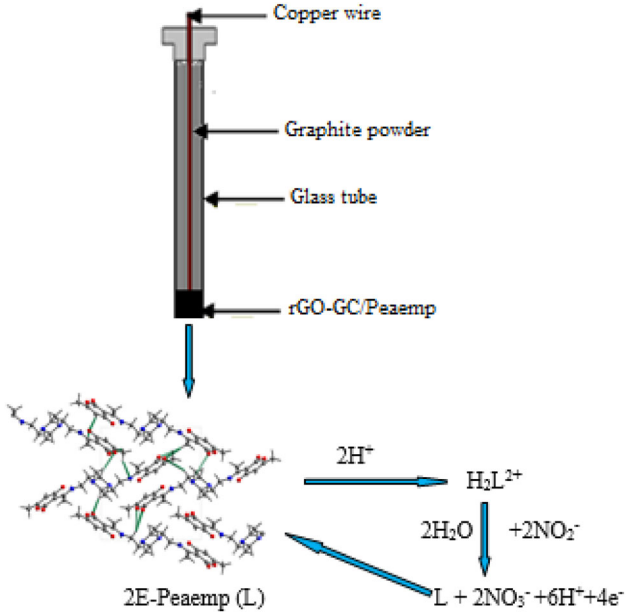

Scheme 2. Schematic representation of the modified electrode (rGO-GC/2E-Peaemp) and the oxidation mechanism of nitrite ions.

the oxidation peak current increases linearly with increasing the nitrite concentration in the range of 0–4.0 mM in neutral medium.

The recorded voltammograms showed a well-defined anode wave corresponding to the electronic oxidation process of the conversion of nitrite NO_2^- to nitrate NO_3^-on the surface of the modified electrode, with an oxidation peak potential observed between 0.80 and 0.85 V,[53,54] according to equation 1:

$$NO_2^- + H_2O \rightarrow NO_3^- + 2H^+ + 2e^- \quad (1)$$

The electrocatalytic characteristics of this ligand towards nitrite oxidation are due to the presence of two amino groups (NH) that will react with H^+ which produced during the conversion of nitrite ions to nitrates according to equation 2:

$$L + 2H^+ \rightarrow H_2L^{2+} \quad (2)$$

Combining (1) and (2), the overall catalytic mechanism is given in the following reaction (Scheme 2):

$$2NO_2^- + H_2L^{2+} + 2H_2O \rightarrow 2NO_3^- + L + 6H^+ + 4e^- \quad (3)$$

The limit of detection (LOD) is defined as the concentration value that generates an electrical signal at least three times the amplitude of the background noise. LOD is determined from the calibration plot of the current intensity versus nitrite concentration $\left(i = a \times \left[NO_2^-\right] + b\right)$ (Figure 4b) using $LOD = \frac{3S}{m}$ formula, where S is the standard deviation of the blank signal and m is the slope of the linear regression equation, respectively. Reporting $i = f\,[NO_2^-]$, the linear equation can be defined as: $i=360.881[NO_2^-]+0.121$ with a correlation coefficient of $R^2 = 0.993$. Based on these electrochemical results, the rGO-GC/2E-Peaemp modified electrode exhibits enhanced electrochemical activity in PBS (pH = 7) with low detection limit (LOD = 0.83 μM). Thus, our modified electrode is more suitable for the determination of nitrite. Indeed, 2E-Peaemp exhibits a better electrocatalytic activity towards nitrite oxidation compared to that previously reported in the literature.[56–58] The limit of detection calculated in the comparable concentration range (0∼4 mM) around neutral pH medium are summarized in Table 2.

To prove the precision of our modified electrode in 0.1 M PBS solution, the stability of the modified electrode (rGO-GC/2E-Peaemp) was tested by detecting 0.001 M NO_2^- (three replicate measurements) after 3 months of storage at 4 °C (Figure S8a, Supplementary Information). It was found that the relative standard deviation (RSD%) of the current response of NO_2^- was about 5.9%. In addition, the reproducibility of the sensor was estimated by detecting 0.001 M NO_2^- with five rGO-GC/2E-Peaemp modified electrodes prepared under the same conditions of measurement. By means of calculations founded upon Figure S8b, Supplementary Information

Table 2. Comparison of the performance of some different modified electrodes towards nitrite detection in the comparable concentration range around neutral pH medium.

Electrode materials	Linear range (mM)	LOD (μM)	Reference
GR/Poly(nBA)	0.05–5.00	30	[56]
TOSC-MoS_2/GCE	0.006–4.20	2	[57]
Myoglobin on LaF_3-doped CeO_2 and ionic liquid composite film	0.005–4.65	2	[58]
rGO-GC/2E-Peaemp	0–4.0	0.83	This work

GR: graphene; Poly(nBA): poly(*n*-butyl acrylate; TOSC: TEMPO oxidized straw cellulose; TEMPO: 2, 2, 6, 6-tetramethylpiperidine-1-oxyl; MoS_2: molybdenum disulfide; GCE: Glassy carbon electrode; LaF_3: Lanthanum trifluoride; CeO_2: Cerium oxide; rGO: reduced graphene oxide.

the result showed that the relative standard deviation (RSD%) of the current response of NO_2^- was about 4.18%.

4. Conclusions

In summary, this work reported synthesis, spectroscopic characterization (ESI-MS, ATR, NMR and UV-Visible), crystal structure (XRD) and optimized structure (DFT) of 2E-Peaemp. The results of single-crystal X-ray diffraction analysis of this compound showed that the ligand crystallizes in monoclinic crystal system (space group: P 2_1/c) and the structure of these crystals is stabilized by hydrogen bonding network and also by van der Waals interactions. Density functional theory (DFT) study showed a good agreement with XRD results. The HOMO-LUMO energy gap and other related parameters revealed that the ligand exhibits high chemical reactivity and low kinetic stability. The two NH groups of the ligand play a key role in the reaction process of this compound with nitrite ions, and this recognition allows easy detection of NO_2^- using rGO-GC/2E-Peaemp modified electrode. In addition, the modified electrode (rGO-GC/2E-Peaemp) exhibits a low detection limit (0.83 μM) for nitrite sensing in a wide concentration range of 0 M to 4 mM at pH = 7.

Supplementary Information (SI)

Crystallographic data for the structural analysis have been deposited at the Cambridge Crystallographic Data Center, CCDC No 1980136. These data can be obtained via https://www.ccdc.cam.ac.uk, e-mail:deposit@ccdc.cam.ac.uk. Plots of ESI-MS, ATR-FTIR, ^{1}H NMR and ^{13}C NMR, 2D NMR, UV-Visible spectra, SEM image and Cyclic Voltammogram of 2E-Peaemp and stability of the modified electrode are reported in Figures S1–S8. Crystal data, structure parameters, the fractional coordinates, isotropic and anisotropic displacement parameters and hydrogen bonding geometry for 2E-Peaemp are summarized in Tables S1–S5. Supplementary Information is available at www.ias.ac.in/chemsci.

Acknowledgements

The authors would like to acknowledge the MESRS Algerian Ministry and Directorate-General for Scientific Research and Technological Development (Algeria) for supporting the present research.

References

1. Mao S, Han X, Li C, Xu Y, Shen K, Shi X and Wu H 2018 Cu(I) complexes regulated by N-heterocyclic ligands: Syntheses, structures, fluorescence and electrochemical properties *Spectrochim. Acta Part A* **203** 408
2. De Souza I P, Machado B P, Carvalho A B, Binatti I, Krambrock K, Molphy Z, Kellett A, Pereira-Maia E C and Caldeira P P S 2019 Exploring the DNA binding, oxidative cleavage, and cytotoxic properties of new ternary copper(II) compounds containing 4-aminoantipyrine and N,N-heterocyclic co-ligands *J. Mol. Struct.* **1178** 18
3. Heer P K K S, Khot K M and Gaikar V G 2016 Development of polystyrene adsorbents functionalized with heterocyclic ligands for selective adsorption of CO_2 from CH_4 and N_2 *Sep. Purif. Technol.* **158** 212
4. Rubino S, Pibiri I, Minacori C, Alduina R, Di Stefano V, Orecchio S, Buscemi S, Girasolo M A, Tesoriere L and Attanzio A 2018 Synthesis, structural characterization, anti-proliferative and antimicrobial activity of binuclear and mononuclear Pt(II) complexes with perfluoroalkyl-heterocyclic ligands *Inorg. Chim. Acta* **483** 180
5. Al-Adilee K and Kyhoiesh H A K 2017 Preparation and identification of some metal complexes with new heterocyclic azo dye ligand 2-[2$^-$- (1- Hydroxy -4- Chloro phenyl) azo]- imidazole and their spectral and thermal studies *J. Mol. Struct.* **1137** 160
6. Hemmert C, Fabié A, Fabre A, Benoit-Vical F and Gornitzka H 2013 Synthesis, structures, and antimalarial activities of some silver(I), gold(I) and gold(III) complexes involving *N*-heterocyclic carbene ligands *Eur. J. Med. Chem.* **60** 64

7. Ait-Ramdane-Terbouche C, Terbouche A, Khalfaoui M, Douib C L, Lakhdari H, Lerari D, Bachari K, Mezaoui D, Guegan J P and Hauchard D 2018 Synthesis, characterization and molecular modeling of binuclear Pd(II) and Ir(IV) complexes with bis [4-hydroxy-6-methyl-{(1E)-N-[2-(ethylamino)ethyl]ethanimidoyl}-2H-pyran-2-one]: Application to detection of glucose *J. Mol. Struct.* **1170** 119
8. Shukla S N, Gaur P and Chaurasia C 2019 Studies on heterocyclic anchored Cu(II) complexes with ONO pincer type donor ligand as an efficient biomimetic and anticorrosion agent *J. Mol. Struct.* **1186** 345
9. Bayar I, Khedhiri L, Fezai R, da Silva P S P, Silva M R and Ben Nasr C 2019 A hybrid perchlorate with a low band gap: Crystal structure, physicochemical characterization and Hirshfeld surfaces study *J. Mol. Struct.* **1181** 300
10. Mateescu C, Wikete C, Costisor O, Bouet G and Khan M A 2005 Protonation behaviour of *N*,*N*′-piperazine-dipropionic acid *C. R. Chim.* **8** 1149
11. Ferreira S B and Kaiser C R 2012 Pyrazine Derivatives: A Patent Review (2008 - Present) *Expert Opin. Ther. Pat.* **22** 1033
12. Rubino S, Pibiri I, Minacori C, Alduin R, Di Stefano V, Orecchio S, Buscemi S, Girasolo M A, Tesoriere L and Attanzio A 2018 Synthesis, structural characterization, anti-proliferative and antimicrobial activity of binuclear and mononuclear Pt(II) complexes with perfluoroalkyl-heterocyclic ligands *Inorg. Chim. Acta* **483** 180
13. Shukla S N, Gaur P and Chaurasia B 2019 Studies on heterocyclic anchored Cu (II) complexes with ONO pincer type donor ligand as an efficient biomimetic and anticorrosion agent *J. Mol. Struct.* **1186** 345
14. Macaev F, Ribkovskaia Z, Pogrebnoi S, Boldescu V, Rusu G, Shvets N, Dimoglo A, Geronikaki A and Reynolds R 2011 The structure–antituberculosis activity relationships study in a series of 5-aryl-2-thio-1,3,4-oxadiazole derivatives *Bioorg. Med. Chem.* **19** 6792
15. Vieth M, Siegel M G, Higgs R E, Watson I A, Robertson D H, Savin K A, Durst G L and Hipskind P A 2004 Characteristic Physical Properties and Structural Fragments of Marketed Oral Drugs *J. Med. Chem.* **47** 224
16. Nordstrøm L U and Madsen R 2007 Iridium catalysed synthesis of piperazines from diols *Chem. Comm.* **47** 5034
17. Gao H, Zhang X, Pu X J, Zheng X, Liu B, Rao G X, Wan C P and Mao Z W 2019 2-Benzoylbenzofuran derivatives possessing piperazine linker as anticancer agents *Bioorg. Med. Chem. Lett.* **29** 806
18. Haga N, Ishibashi T, Hara A and Abiko Y 1985 Effect of NCO-700, an Inhibitor of Protease, on Myocardial pH Decreased by Coronary Occlusion in Dogs *Pharmacology* **31** 208
19. Swindell E P, Ugolkov A, Freguia C, Dubrovskyi O, Hankins P L, Yang J, Raizer J J, Chandler J P, James C D, Mazar A P and O'Halloran T V 2015 Liposomes containing piperazine compounds inhibit tumor growth in a patient-derived xenograft model of glioblastoma multiforme *J. Cancer Res.* **75** 18
20. Patil M, Poyil A N, Joshi S D, Patil S A and Bugarin A 2019 Design, synthesis, and molecular docking study of new piperazine derivative as potential antimicrobial agents *Bioorg. Chem.* **92** 103
21. Koparde S, Hosamani K M, Kulkarni V and Joshi S D 2018 Synthesis of coumarin-piperazine derivatives as potent anti-microbial and anti-inflammatory agents, and molecular docking studies *Chem. Data Collect.* **15-16** 197
22. Ryckebusch A, Poulain R D, Maes L, Debreu-Fontaine M A, Mouray E, Grellier P and Sergheraert C 2003 Synthesis and in Vitro and in Vivo Antimalarial Activity of N^1-(7-Chloro-4-quinolyl)-1,4-bis(3-aminopropyl)piperazine Derivatives *J. Med. Chem.* **46** 542
23. Shaquiquzzaman M, Verma G, Marella A, Akhter M, Akhtar W, Khan M F, Tasneem S and Alam M M 2015 Piperazine scaffold: A remarkable tool in generation of diverse pharmacological agents *Eur. J. Med. Chem.* **102** 487
24. Gu Z S, Zhou A N, Xiao Y, Zhang Q W and Li J Q 2018 Synthesis and Antidepressant-Like Activity of Novel Aralkyl Piperazine Derivatives Targeting SSRI/5-HT_{1A}/5-HT_7 *Eur. J. Med. Chem.* **144** 701
25. Chaudhary P, Kumar R, Verma A K, Singh D, Yadav V, Chhillar A K, Sharma G L and Chandra R 2006 Synthesis and antimicrobial activity of *N*-alkyl and *N*-aryl piperazine derivatives *Bioorg. Med. Chem.* **14** 1819
26. Popova A, Christov M and Zwetanova A 2007 Effect of the molecular structure on the inhibitor properties of azoles on mild steel corrosion in 1 M hydrochloric acid *Corros. Sci.* **49** 2131
27. Issa R M, Awad M K and Atlam F M 2008 Quantum chemical studies on the inhibition of corrosion of copper surface by substituted uracils *App. Surf. Sci.* **255** 2433
28. Masoud M S, Awad M K, Shaker M A and El-Tahawy M T 2010 The role of structural chemistry in the inhibitive performance of some aminopyrimidines on the corrosion of steel *Corros. Sci.* **52** 2387
29. Dagci K and Alanyalioglu M 2013 Electrochemical preparation of polymeric films of pyronin Y and its electrolcatalytic properties for amperometric detection of nitrite *J. Electroanal. Chem.* **711** 17
30. Yaqoob M, Biot B F, Nabi A and Worsfold P G 2012 Determination of nitrate and nitrite in freshwaters using flow-injection with luminol chemiluminescence detection *Luminescence* **27** 419
31. Cheng S Y, Yang X N, Tao Z, Wei L T, Zhao W W, Jiang D F, Jin Y M, Gao J and Ma P H 2020 Trans-4-[4-(Dimethyla,ino) styryl]-1-methylpyridinium iodide @ cyclopentanocucurbit [6] uril as fluorescent probe for anion recognition *J. Chem. Sci.* **132** 60
32. Chowdhury A R, Ghosh P, Kr.Saha S, Mitra P and Banerjee P 2014 Exploratory studies towards various anion recognition chemistry by two different sized cleft shaped organic ligands *Spectrochim. Acta Part A* **124** 492
33. Wang Q H, Yu L J, Liu Y, Lin L, Lu R G, Zhu J P, He L and Lu Z L 2017 Methods for the detection and determination of nitrite and nitrate: A review *Talanta* **165** 709
34. Yilong Z, Dean Z and Daoliang L 2015 Electrochemical and Other Methods for Detection and Determination of Dissolved Nitrite: A Review *Int. J. Electrochem. Sci.* **10** 1144

35. Zhang S X, Peng R, Jiang R, Chai X S and Barnes D G 2018 A high-throughput headspace gas chromatographic technique for the determination of nitrite content in water samples *J. Chromatog. A* **1538** 104
36. Singh P, Singh M K, Beg Y R and Nishad G R 2019 A review on spectroscopic methods for determination of nitrite and nitrate in environmental samples *Talanta* **191** 364
37. Lo H S, Lo K W, Yeung C F and Wong C Y 2017 Rapid Visual and Spectrophotometric Nitrite Detection by Cyclometalated Ruthenium Complex *Anal. Chim. Acta* **990** 135
38. Li X, Ping J and Ying Y 2019 Recent developments in carbon nanomaterial-enabled electrochemical sensors for nitrite detection *Trends Anal. Chem.* **113** 1
39. Lu L 2019 Highly sensitive detection of nitrite at a novel electrochemical sensor based on mutually stabilized Pt nanoclusters doped CoO nanohybrid *Sens. Actuat. B: Chem.* **281** 182
40. Elsayed S A, Noufal A M and El-Hendawy A M 2017 Synthesis, structural characterization and antioxidant activity of some vanadium(IV), Mo(VI)/(IV) and Ru(II) complexes of pyridoxal Schiff base derivatives *J. Mol. Struct.* **1144** 120
41. Gaber M, Awad M K and Atlam F M 2018 Pd (II) complexes of bidentate chalcone ligands: Synthesis, spectral, thermal, antitumor, antioxidant, antimicrobial, DFT and SAR studies *J. Mol. Struct.* **1160** 348
42. Raman N, Joseph J, Sakthivel A and Jeyamurugan R 2009 Synthesis, structural characterization and antimicrobial studies of novel schiff base copper(ii) complexes *J. Chil. Chem. Soc.* **54** 354
43. Saritha S R, Anitha L, Layana S R, Sudarsanakumar M R, Joe I H, Manimaran D and Siji V L 2019 Spectral, structural and theoretical studies of α-methyl *trans* cinnamaldehyde semicarbazone *J. Mol. Struct.* **1182** 329
44. Laricheva Y A, Gushchin A L, Abramov P A and Sokolov M N 2018 Novel mixed-metal cubane-type $\{Mo_3NiS_4\}$ and $\{Mo_3PdS_4\}$ clusters coordinated with 2,2′-bipyridine type ligands *Polyhedron* **154** 202
45. Demircioğlu Z, Ersanli C C, Kantar G K and Şaşmaz S 2019 Spectroscopic, Hirshfeld surface, X-ray diffraction methodologies and local & global chemical activity calculations of 5-(2-methoxy-4-(prop-1-en-1-yl)phenoxy)pyrazine-2,3-dicarbonitrile *J. Mol. Struct.* **1181** 25
46. Dayan O, Tercan M and Ozdemir N 2016 Syntheses and molecular structures of novel Ru(II) complexes with bidentate benzimidazole based ligands and their catalytic efficiency for oxidation of benzyl alcohol *J. Mol. Struct.* **1123** 35
47. Frisch M J, Trucks G W, Schlegel H B, Scuseria G E, Robb M A, Cheeseman J R, Scalmani G, Barone V, Mennucci B, Petersson G A, Nakatsuji H, Caricato M, Li X, Hratchian H P, Izmaylov A F, Bloino J, Zheng G, Sonnenberg J L, Hada M, Ehara M, Toyota K, Fukuda R, Hasegawa J, Ishida M, Nakajima T, Honda Y, Kitao O, Nakai H, Vreven T, Montgomery J A, Peralta J E, Ogliaro F, Bearpark M, Heyd J J, Brothers E, Kudin K N, Staroverov V N, Kobayashi R, Normand J, Raghavachari K, Rendell A, Burant J C, Iyengar S S, Tomasi J, Cossi M, Rega N, Millam J M, Klene M, Knox J E, Cross J B, Bakken V, Adamo C, Jaramillo J, Gomperts R, Stratmann R E, Yazyev O, Austin A J, Cammi R, Pomelli C, Ochterski J W, Martin R L, Morokuma K, Zakrzewski V G, Voth G A, Salvador P, Dannenberg J J, Dapprich S, Daniels A D, Farkas O, Foresman J B, Ortiz J V, Cioslowski J, Fox D J, 2009 *Gaussian Inc*, Wallingford C T.
48. Aouad M R, Messali M, Rezki N, Said M A, Lentz D, Zubaydi L and Warad I 2019 Hydrophobic pocket docking, double-proton prototropic tautomerism in contradiction to single-proton transfer in thione ⇔ thiol Schiff base with triazole-thione moiety: Green synthesis, XRD and DFT-analysis *J. Mol. Struct.* **1180** 455
49. Okulik N and Jubert A H 2005 Theoretical Analysis of the Reactive Sites of Non–steroidal Anti–inflammatory Drugs *J. Mol. Des.* **4** 17
50. Scott A P and Radom L 1996 Harmonic Vibrational Frequencies: An Evaluation of Hartree–Fock, Møller–Plesset, Quadratic Configuration Interaction, Density Functional Theory, and Semiempirical Scale Factors *J. Phys. Chem.* **100** 16502
51. Kosar B and Albayrak C 2011 Spectroscopic investigations and quantum chemical computational study of (*E*)-4-methoxy-2-[(p-tolylimino)methyl]phenol *Spectrochim. Acta A: Mol. Biomol. Spectrosc.* **78** 160
52. Terbouche A, Ait-Ramdane-Terbouche C, Bendjilali Z, Berriah H, Lakhdari H, Lerari D, Bachari K, Mezaoui D, Bensiradj N E H, Guegan J P and Hauchard D 2018 Synthesis, spectral characterization, molecular modeling, antibacterial and antioxidant activities and stability study of binuclear Pd(II) and Ru(III) complexes with novel bis-[1-(2-[(2-hydroxynaphthalen-1-yl)methylidene]amino}ethyl)-1-ethyl-3-phenylthiourea] ligand: Application to detection of cholesterol *Spectrochim. Acta A* **205** 146
53. Bartolome J P and Fragoso A 2017 Electrochemical detection of nitrite and ascorbic acid at glassy carbon electrodes modified with carbon nano-onions bearing electroactive moieties *Inorg. Chim. Acta* **468** 223
54. Shaikh A, Kr Singh B and Parida S 2019 Natural oil derived carbon nano-onions as a sensitive electrocatalyst for nitrite determination *Mater. Chem. Phys.* **235** 121744
55. Eguílaz M, Agüí L, Yáñez-Sedeño P and Pingarrón J M 2010 A biosensor based on cytochrome *c* immobilization on a poly-3-methylthiophene/multi-walled carbon nanotubes hybrid-modified electrode. Application to the electrochemical determination of nitrite *J. Electroanal. Chem.* **644** 30
56. Raja Jamaluddin R Z A, Yook Heng L, Tan L L and Chong K F 2018 Electrochemical Biosensor for Nitrite Based on Polyacrylic-Graphene Composite Film With Covalently Immobilized Hemoglobin *Sensors* **18** 1343
57. Wang Q H, Ma S F, Huang H W, Cao A C, Li M F and He L 2016 Highly sensitive and selective spectrofluorimetric determination of nitrite in food products with a novel fluorogenic probe *Food Control* **63** 117
58. Dong S, Li N, Huang T, Tang H and Zheng J 2012 Myoglobin immobilized on LaF_3 doped CeO_2 and ionic liquid composite film for nitrite biosensor *Sens. Actuat. B* **173** 704